Tectonophysics 608 (2013) 1086–1093

Contents lists available at ScienceDirect

Tectonophysics

journal homepage: www.elsevier.com/locate/tecto

Electrical conductivity of $Alm_{82}Py_{15}Grs_3$ almandine-rich garnet determined by impedance spectroscopy at high temperatures and high pressures

Lidong Dai [a], Heping Li [a,*], Haiying Hu [a], Jianjun Jiang [a,b], Keshi Hui [a,b], Shuangming Shan [a]

[a] Laboratory for High Temperature and High Pressure Study of the Earth's Interior, Institute of Geochemistry, Chinese Academy of Sciences, Guiyang, Guizhou 550002, China
[b] Graduate School of Chinese Academy of Sciences, Beijing 100039, China

ARTICLE INFO

Article history:
Received 12 April 2013
Received in revised form 29 June 2013
Accepted 4 July 2013
Available online 11 July 2013

Keywords:
Electrical conductivity
almandine-rich garnet
oxygen fugacity
high pressure

ABSTRACT

Under conditions of 1.0 ~ 3.0 GPa, 973 ~ 1273 K and frequency range from 10^{-2} to 10^6 Hz, the electrical conductivity of Fe-rich garnet single crystal is measured by virtue of YJ-3000 t multi-anvil high-pressure apparatus and Solartron-1260 Impedance/Gain-phase Analyzer. A series of solid oxygen buffers including $Fe_3O_4 + Fe_2O_3$, $Ni + NiO$, $Fe + Fe_3O_4$, $Fe + FeO$ and $Mo + MoO_2$ are chosen to control oxygen fugacity. Two branches of impedance spectra are obtained in the complex impedance plane, one (10^2-10^6 Hz) showing a semicircular arc originated from the origin in the Nyquist and Bode diagram, another small tail in the low frequency of 10^{-2}-10^2 Hz. Experimental results show that with the rise of temperature (T), electrical conductivity (σ) tends to increase, and Log σ and $1/T$ satisfies the Arrhenius relation. Under control of a $Ni + NiO$ oxygen buffer, with the rise of pressure, electrical conductivity decreases, and the pre-exponential factor also reduces, while the activation enthalpy rises, activation energy and activation volume of charge carriers are determined as 1.29 ± 0.12 eV and 2.01 ± 0.57 cm^3/mol, respectively. The dominant electrical conduction mechanism of anhydrous almandine-rich garnet is the $Fe^{2+} \rightarrow Fe^{3+}$ hopping of small polaron. At 3.0 GPa, electrical conductivity of almandine-rich garnet increases with increasing oxygen fugacity. The electrical conductivity of this sample can be represented by the relation $Log_{10}\sigma = (2.67 \pm 0.05) + (0.054 \pm 0.003)\tilde{n}\log_{10}f_{O_2} + \frac{(-5446 \pm 68)}{T}$, where f_{O_2} is the oxygen fugacity (bar) and T is the absolute temperature (K). At a typical temperature and pressure in the upper mantle, the influence of oxygen fugacity is substantial.

1. Introduction

The *in-situ* laboratory-based electrical conductivity measurements of minerals and rocks at relevant temperatures and pressures can be applied to the interpretation of geophysical observation results on magnetotelluric (MT) and geomagnetic deep sounding (GDS) (e.g., Evans, 2012; Ferri et al., 2013; Fuji-ta et al., 2004, 2007a, b, 2011; Hu et al., 2011, 2013; Jones et al., 2009, 2012; Kelbert et al., 2009; Poe et al., 2010, 2012; Pommier, in press; Pommier and Le-Trong, 2011; Pommier et al., 2010a, b; Selway, 2013; Wang and Karato, 2013; Wang et al., 2006, 2008, 2010). On the other hand, results of experimental studies of the electrical conductivity of minerals and rocks at high T and P can be used to infer the physical and chemical properties of the Earth's interior, such as temperature distribution, thermodynamic structure, partial melting, point defect chemistry, mineralogical composition, element chemical migration, electronic spin transition and water content of the Earth and other planets' interior (e.g., Gaillard et al., 2008; Karato, 2011a, b; Karato and Wang, 2013; Laštovičková, 1991; Ni et al., 2011a, b; Nover, 2005; Xu and McCammon, 2002; Xu and Shankland, 1999; Xu et al., 1998a, b; Xu et al., 2000a, 2000b; Yang, 2011; Yang, 2012; Yang and Heidelbach, 2012; Yang and McCammon, 2012; Yang et al., 2011; Yang et al., 2012; Yoshino, 2010; Zhang et al., 2006, 2012; Zhou et al., 2011).

Garnet is the general term used for garnet-group minerals represented by the chemical formula of A_3B_2 $[SiO_4]_3$, in which A stands for divalent cations such as Mg^{2+}, Fe^{2+}, Mn^{2+} or Ca^{2+} and B stands for Al^{3+}, Fe^{3+}, Cr^{3+}, V^{3+}, Ti^{4+} or Zr^{4+}. Due to their similar characteristics in ionic radius, the B cations are prone to isomorphic substitution; thus, garnet minerals are divided into two subgroups of pyralspite garnets $[(Mg, Fe, Mn)_3Al_2[SiO_4]_3]$ and ugrandite garnets $[Ca_3(Al, Fe, Cr, Ti, V, Zr)_2(SiO_4)_3]$. Garnet samples of various compositions are indicative of the typomorphic property (their formation conditions and genetic features), which facilitates the identification of their various genetic types (e.g., ultrabasic rock, granite, pegmatite, skarn and regional metamorphic rock) based on intrinsic characteristic elements (Mookherjee and Karato, 2010). Garnet has the widest depth distribution in the mantle. In view of its own complex chemical

* Corresponding author. Tel.: +86 851 5895159; fax: +86 851 5891749.
E-mail address: hepingli_2007@hotmail.com (H. Li).

0040-1951/$ – see front matter © 2013 Elsevier B.V. All rights reserved.
http://dx.doi.org/10.1016/j.tecto.2013.07.004

composition and structure stability, compared with electrical conductivity measurements on other representative rock-forming minerals such as olivine, orthopyroxene, clinopyroxene, wadsleyite and ringwoodite that only exist in the limited depth range in the upper mantle and the transition zone, in-situ experimental measurement of electrical conductivity for garnet at high pressure becomes more important (Dai and Karato, 2009a, b, c; Dai et al., 2008a, b, 2009, 2010, 2012; Du Frane and Tyburczy, 2012; Du Frane et al., 2005; Huang et al., 2005, 2006; Karato and Dai, 2009; Romano et al., 2006, 2009). As such, the knowledge of its electrical property is crucial to interpret the conductivity-depth profile of the earth's interior.

Electrical conductivity measurements on the natural majorite, almandine-rich and pyrope-rich garnets have been extensively performed (e.g., Dai et al., 2009, 2012; Kavner et al., 1995; Romano et al., 2006; Xu and Shankland, 1999). Kavner et al. (1995) measured electrical conductivity of majorite garnet under conditions of atmospheric pressure and 20–100 °C to apply mantle conditions. However, it is difficult to extrapolate these results to high pressure and temperature conditions in the Earth's mantle. Xu and Shankland (1999) measured electrical conductivities within orthopyroxene, clinopyroxene, and garnet + ilmenite stability filed with the same starting material San Carlos orthopyroxene (the corresponding chemical composition is $(Mg_{0.92}Fe_{0.08})$ SiO_3 + 2.89 wt% Al_2O_3) at conditions of 1000–1400 °C and 5–21 GPa. However, the recovered sample after electrical conductivity was a mixture of ilmenite and garnet. Romano et al. (2006) measured electrical conductivities of synthetic polycrystalline garnets with different chemical compositions from almandine ($Fe_3Al_2Si_3O_{12}$) to pyrope ($Mg_3Al_2Si_3O_{12}$) at 10–19 GPa and 300–1700 °C and confirmed the important influence of Mg/Fe ratio on garnet conductivity. In addition, recently, Dai et al. (2009a, 2012) showed that electrical conductivities of hydrous and anhydrous pyrope-rich garnet were dependent on water content (from less than 10 to 7000 $H/10^6$ Si) and oxygen partial pressure at conditions of 1.0-16 GPa and 873–1473 K. However, as another crucial endmember of garnet group, the effect of oxygen fugacity on the electrical conductivity of almandine has never been reported till now at high temperature and high pressure.

In this study, we determined the electrical conductivity of almandine-rich garnet at the frequency range from 0.01 Hz to 1 MHz using the impedance spectroscopy. A series of characteristic parameters including the pre-exponential factor, activation energy and activation volume have been obtained. At the pressure of 3.0 GPa, a functional relation model describing the electrical conductivity of almandine-rich garnet as a function of oxygen fugacity was constructed. The conduction mechanism of almandine-rich garnet has also been discussed in details.

2. Experimental procedures

2.1. Sample preparation

Dry gem-grade almandine-rich garnet single crystals were collected from the basaltic xenoliths in the Altai region of Xinjiang Uyghur Autonomous Region in China. The surfaces of samples were fresh, nonfractured, nonoxidized, rhombic trioctahedron crystallographic structure without any evidences of major alternation. The chemical compositions of the samples were determined by virtue of the EPMA-1600 electron microprobe at the State Key Laboratory of Ore Deposit Geochemistry, Institute of Geochemistry, Chinese Academy of Sciences and listed in Table 1. In order to check the phase state during electrical conductivity measurements, a typical quenched sample image observation after EC measurement was investigated by an optical microscope of a plane-polarized reflected light and a back-scattered electron image derived from the analysis of scanning electronic microscope as shown in Fig. 1>. Firstly, almandine-rich garnets single crystals were cut and polished into a cylinder of φ 4.5 mm × 5.0 mm with the ultrasonic drill and diamond slice; then, the samples were cleaned with the deionized distilled water, alcohol and acetone in turn. The samples were baked for 48 hrs in a 473 K vacuum drying oven in order to remove the adsorbed water on the surfaces of the samples.

Table 1
Chemical compositions of the starting material.

Compositions	Contents
MgO	3.71
NiO	0.02
Al_2O_3	18.69
SiO2	38.37
CaO	1.05
TiO_2	0.06
Cr_2O_3	0.07
K_2O	0.03
Na_2O	0.07
MnO	1.24
FeO	37.13
Total	100.44

2.2. FT-IR measurement

In order to determine the water content of the samples, the infrared spectra of samples were obtained at wavenumbers from 1000 to 7000 cm^{-1} both before and after each conductivity experiment in the Department of Geology and Geophysics, Kline Geological Lab, Yale University, New Haven, Connecticut, USA. Detailed procedures for the FT-IR analysis are described as follows. Firstly, the sample was cut and polished in double sides up to less than 120 μm thickness

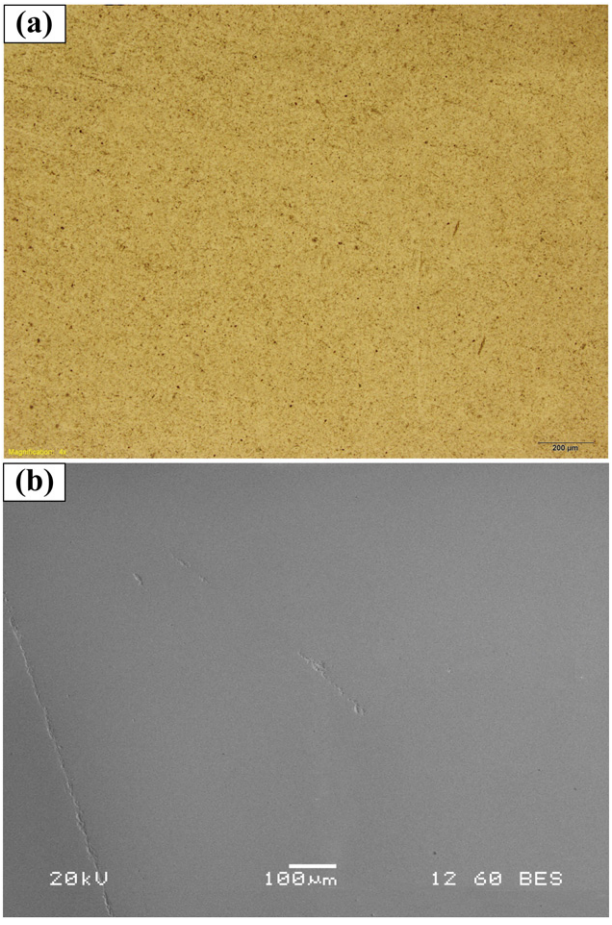

Fig. 1. Representative microscopic images of quenched almandine-rich garnet after electrical conductivity measurement derived from the plane-polarized reflected light (a) and the back-scattered electron images derived from the analysis of scanning electronic microscope (b).

using a Vibromet-2 Diamond Polisher and Ecomet-4 Diamond Polisher. The measurements were performed by a Fourier transform infrared spectrum analyzer (FT-IR, BIORAD, Varian 600 UMA). The IR absorption spectra of samples were measured by the unpolarized radiation with a KI beam splitter, a MCT detector and a Mid-IR light source. Two hundred fifty-six scans were collected for each spectrum. Apertures of 80 × 80 μm^2 square were applied for the measurements of selected sample areas. At least six spectra were conducted on the different areas of transparent sample surfaces and made an average value in order to avoid the heterogeneity effect of water distribution. Typical infrared spectra of the acquired samples before and after electrical measurements are shown in Fig. 2.

The water (hydrogen) content of a sample was calculated by the absorption spectrum at a wavenumber range from 3000 to 3750 cm^{-1} using the equation proposed by Paterson (1982),

$$C_{OH} = \frac{B_i}{150\xi}\int \frac{K(\nu)}{(3780-\nu)}d\nu \quad (1)$$

where C_{OH} is the molar concentration of hydroxyl (ppm wt H_2O or H/10^6 Si), B_i is the density factor (cm H/10^6 Si), ξ is the orientation factor (1/2), and $K(\nu)$ is the absorption coefficient in cm^{-1} at a wavenumber ν in cm^{-1}. The integration was conducted at a wavenumber range from 3000 to 3750 cm^{-1}. The water contents before and after conductivity measurements are less than ~3 H/10^6 Si and ~6 H/10^6 Si respectively, and thus, we call them as really "dry" almandine-rich garnet. The variation of water content during the electrical conductivity measurements of dry sample is not more than 20 %.

2.3. Oxygen buffer control

The solid oxygen fugacity buffers were obtained by homogenously mixing the 99 % high-purity powders of metals (e.g. Ni, Fe and Mo) and its corresponding metallic oxides (e.g. NiO, FeO, Fe_2O_3, Fe_3O_4, and MoO_2). The following reactions are employed to buffer the oxygen fugacity:

$$MH: 4Fe_3O_4 + O_2 \rightleftharpoons 6Fe_2O_3 \quad (2)$$

$$NNO: 2Ni + O_2 \rightleftharpoons 2NiO \quad (3)$$

$$IM: 3Fe + 2O_2 \rightleftharpoons Fe_3O_4 \quad (4)$$

$$IW: 2Fe + O_2 \rightleftharpoons 2FeO \quad (5)$$

$$MMO: Mo + O_2 \rightleftharpoons MoO_2 \quad (6)$$

For each given solid buffer, oxygen fugacity values are a function of pressure and temperature which can be expressed as (Chou, 1978; Chou and Eugster, 1976):

$$\text{Log } f_{O_2} = -\frac{\alpha}{T} + \beta + \gamma\frac{(P-1)}{T} \quad (7)$$

Here, α, β and γ are constants directly related to the standard enthalpy, the standard entropy, and the molar volume variation of the solid combination before and after the balancing buffer reaction; T is the absolute temperature (K), and P is the pressure (atm). The theoretical calculation results of oxygen fugacities for five different solid buffers [Fe_3O_4 + Fe_2O_3 (MH), Ni + NiO (NNO), Fe + Fe_3O_4 (IM), Fe + FeO (IW) and Mo + MoO_2 (MMO)] under conditions of 3.0 GPa and 950–1350 K were shown in Fig. 3. In the typical upper mantle, the oxygen fugacity is inferred to be close to FQM (fayalite-quartz-magnetite) or NNO (nickel-nickel oxide) buffer (Frost and McCammon, 2008; McCammon et al., 2004). Just as the technique described by Dai et al. (2009), the oxygen fugacity is controlled and adjusted by changing the metal-bearing types in the shielding cases, electrodes and their corresponding buffer loops at a predetermined temperature and pressure. In addition, in order to verify the efficiency and accuracy of the solid oxygen buffer, it is crucial to perform the X-ray diffraction analysis on the recovery buffers after electrical conductivity measurements. If two phases for each metal and its corresponding metal oxide coexisted, it indicates that the oxygen fugacity is effectively controlled during the electrical conductivity measurements.

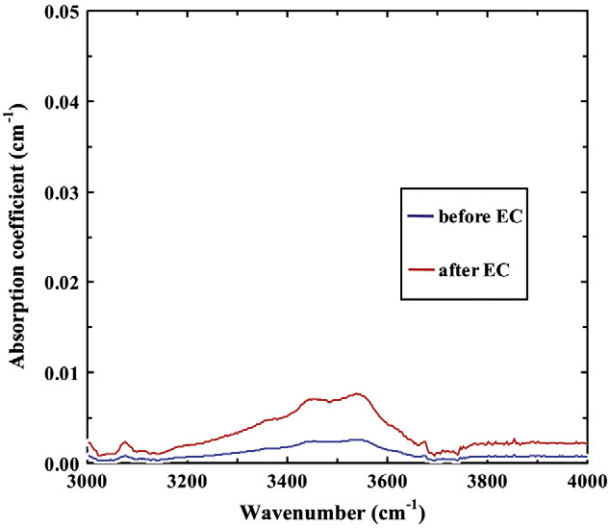

Fig. 2. FT-IR spectra of almandine-rich garnet for the wavenumber range from 3000–4000 cm^{-1} before and after electrical conductivity measurement.

2.4. Impedance measurements

In-situ high-pressure electrical conductivity measurements of samples were performed in the YJ-3000 t multi-anvil press and Solartron-1260 impedance/gain-phase analyzer in the Laboratory for High Temperature and High Pressure Study of the Earth's Interior, Institute of Geochemistry, Chinese Academy of Sciences. A detailed description of the equipment was given previously by Xu et al. (1994) and Liu et al. (2002).

High pressures were generated by six cubic tungsten carbide anvils with a total surface area of 23.4 mm^2. A diagram of the cross-section of

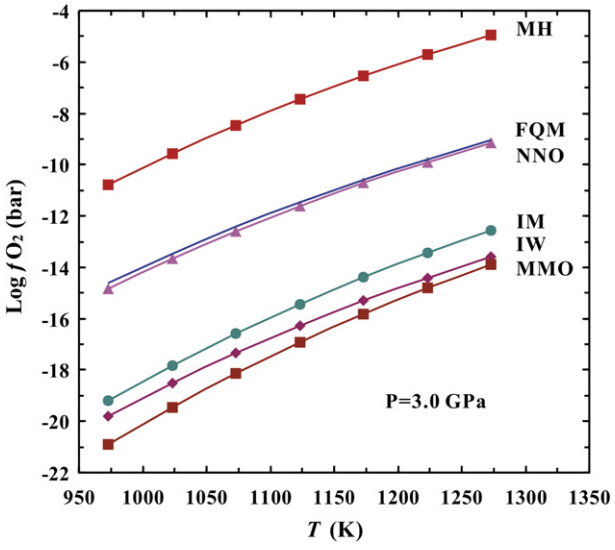

Fig. 3. Temperature dependence of oxygen fugacity for the Fe_3O_4 + Fe_2O_3, Ni + NiO, Fe + Fe_3O_4, Fe + FeO and Mo + MoO_2 buffers at the pressure of 3.0 GPa. Shown together is the oxygen fugacity value of Fayalite + Quartz + Magnetite (FQM).

high-pressure cell assembly for electrical conductivity measurements is shown in Fig. 4. A metal Faraday shielding case that is made of the 0.05 mm metal foil and connected to Earth's ground is installed between the pressure medium and the boron nitride insulation tube, and therefore it can efficiently reduce the temperature gradient inside the sample cell, minimize the current leakage across the pressure medium of pyrophyllite, and as well as prevent the chemical migration between the sample and pressure medium. A cylindrical sample (φ 4.5 mm × 5.0 mm) was placed in the BN insulation tube between two symmetric electrodes of metal buffers. Boron nitride can provide a better insulation material than alumina (Al_2O_3) (Fuji-ta et al., 2007a). Experimental temperature was monitored by a *Pt-Pt$_{90}$Rh$_{10}$* thermocouple. The measurement errors from the temperature and pressure gradients were less than 10 K and 0.1 GPa, respectively. The electrical conductivity measurement errors were estimated at not more than 5 %, and the major error source was determined to be dimensional variations of sample, which are less than 8 %.

The complex impedance spectra measurements were conducted by virtue of the Solartron-1260 impedance/gain-phase analyzer. The sinusoidal alternating current signal voltage was applied within the frequency range from 0.01 Hz to 10^6 Hz during the high temperature and high pressure experiments. Two impedance semicircles were recognized within the high-frequency and low-frequency range, respectively. The sample resistance can be obtained only through fitting high-frequency semicircles when one appropriate equivalent circuit is selected. One typical equivalent circuit that is made up of a series of a parallel constant phase element (CPE) and a resistor was adopted.

3. Results

In the present studies, we have obtained the results of electrical conductivities of natural almandine-rich garnet single crystals ($Alm_{82}Py_{15}Grs_3$) under the conditions of pressures of 1.0-3.0 GPa and temperatures of 973–1273 K, and as well as 3.0 GPa, 973–1273 K, and five different oxygen buffers including WH, NNO, IM, IW and MMO. The frequency range of impedance spectra is 10^{-2}-10^6 Hz.

The representative Nyquist and Bode diagram of complex plane are shown in Figs. 5 and 6 under conditions of 3.0 GPa, 973–1273 K and a NNO oxygen buffer. The results obtained at other conditions are similar to those illustrated. Fig. 5 displays the relationship between the real part (Z') and imaginary part (Z") of complex impedance spectra and satisfy the relation,

$$Z' = |Z|\cos\theta \tag{8}$$

$$Z'' = |Z|\sin\theta \tag{9}$$

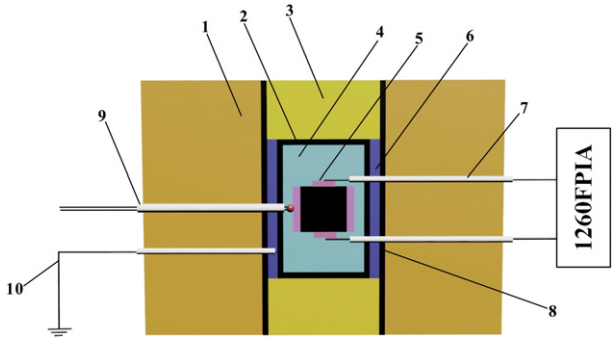

Fig. 4. Experimental assembly for electrical conductivity measurements at high temperature and pressure. 1: Pressure medium (baked to 973 K); 2: Metal shielding cases; 3: Pyrophyllite plug (baked to 1073 K); 4: BN insulation tube; 5: Buffer electrode and ring; 6: Al_2O_3; 7: Electrode lead and Al_2O_3 sleeve; 8: Tri-layers stainless steel heater; 9: *Pt-Pt$_{90}$Rh$_{10}$* thermocouple; 10: Earth line.

Just as discussed by Tyburczy and Roberts (1990), Roberts and Tyburczy (1991), Roberts and Tyburczy (1993a, 1993b, 1994), Roberts and Duba (1995), Roberts et al. (2007), Bagdassarov et al. (2007, 2011a) and Bagdassarov (2011), the high-frequency (102-106 Hz) mechanism of impedance spectra is interpreted as bulk (grain interior) conduction, and the lower-frequency (10-2-102 Hz) mechanism of impedance spectra is attributed to sample-electrode interface polarization effects at a given temperature, pressure and oxygen fugacity condition. From Fig. 5, it is clear that the τC characteristic time constant (or relaxation time, which can be expressed as $R \times C$) can be used to discriminate different conduction mechanisms of a sample. The high-frequency branch of impedance semicircular arc that stands for the bulk conduction process has a relatively low relaxation time, while the lower-frequency branch of impedance small tail that represents the sample-electrode polarization effects has a relatively high relaxation time. With increasing temperature, the electrical conductivity of sample increases and the obvious semi-conductor characteristics is observed at high temperature conditions. Fig. 6 shows the dependence relation of the real part (Z'), the imaginary part (Z''), the magnitude ($|Z|$) and the phase angle (θ) of complex impedance on the frequency.

A representative relationship between electrical conductivity of sample and the inverse temperature under conditions of 1.0-3.0 GPa and a NNO oxygen buffer is illustrated in Fig. 7. The obtained fitted results for electrical conductivity are listed in Table 2. In most cases, the electrical conductivity was obtained in the process of decreasing temperature after the peak temperature was reached. However, in a few runs, the measurements of conductivity were conducted along with decreasing and increasing temperature in order to test the hysteresis. We found no large hysteresis that indicates nearly equilibrium state at each given physical and chemical measurement conditions. The relationship between the electrical conductivity of garnet single crystal and temperature were found to satisfy the Arrhenius linear relation,

$$\sigma = \sigma_0 \exp(-\Delta H/RT) \tag{10}$$

where σ_0 is the pre-exponential factor that is approximately independent temperature (S/m), ΔH is the activation enthalpy (eV), and R is the gas constant (8.3144 dm^3 × kPa/mol/K). The relationship among

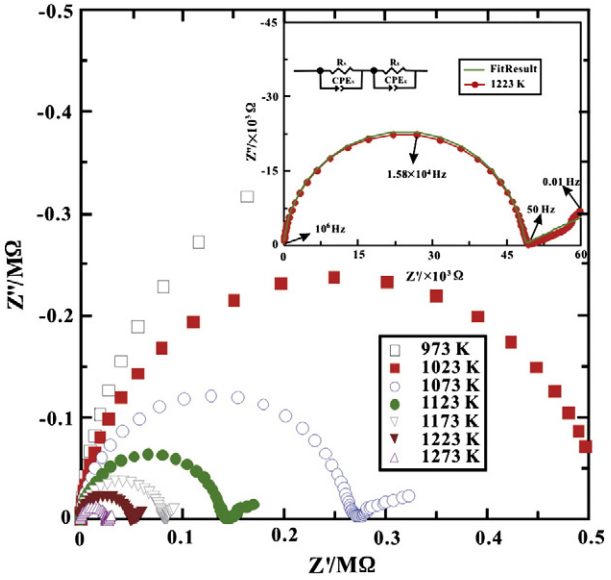

Fig. 5. Nyquist Z' vs. additive inverse Z" plots of the impedance for almandine-rich garnet with the frequency range from 10^{-2} Hz to 1 MHz, obtained under the conditions of 3.0 GPa, 973–1273 K and a NNO buffer. Z' and Z'' represents the real part and imaginary part of complex impedance, respectively.

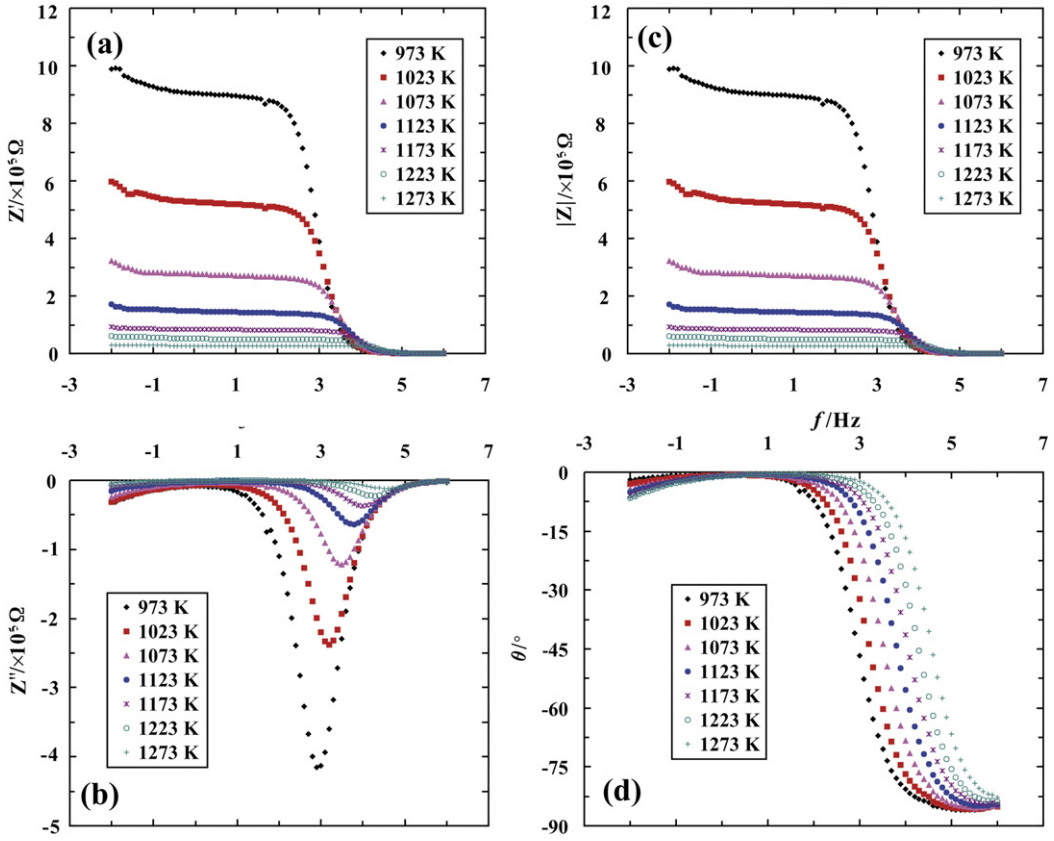

Fig. 6. Bode diagram for almandine-rich garnet with the frequency range from 10^{-2} Hz to 1 MHz, obtained under the conditions of 3.0 GPa, 973–1273 K and a NNO buffer. The dependence of real part (Z'), the imaginary part (Z''), magnitude ($|Z|$) and phase angle (θ) of complex impedance on frequency are shown in Figs (a), (b), (c) and (d), respectively.

activation enthalpy (ΔH), activation energy (ΔU) and activation volume (ΔV) can be represented by the following equation,

$$\Delta H = \Delta U + P \times \Delta V \tag{11}$$

4. Discussion

It is well known that the electrical conductivity of iron-bearing mineral and rock is highly sensitive to the redox conditions. Thus, when we try to apply laboratory-based conductivity data to calculate the upper-mantle profile, it is crucial to take account of the influence of oxygen fugacity fO_2 in the upper mantle. The petrological studies suggest that the oxygen fugacity of the upper mantle lies between IW (iron + wüstite) and FQM (Fayalite + Quartz + Magnetite) buffers, and that the transition zone and lower mantle aO_2 is possibly near to IW buffer (Xu et al., 2000b). And furthermore, in consideration of a nearest FQM oxygen fugacity value in the upper-mantle top listed in Fig. 1, a NNO buffer is selected to explore the pressure effect on the electrical conductivity of almandine-rich garnet. Fig. 7 shows the influence of temperature and pressure on electrical conductivity. The activation energy (ΔE) and activation volume $\left(\Delta V = \left(\frac{\partial \Delta H}{\partial \Delta P}\right) = -\frac{\partial\left(\frac{\partial \ln \sigma}{k\partial T^{-1}}\right)_P}{\partial \Delta P}\right)$ were determined at conditions of 1.0-3.0 GPa, 973–1273 K and a NNO oxygen buffer, yielding values of 1.29 ± 0.12 eV and 2.01 ± 0.57 cm^3/mol, respectively. The present experimental results are in good agreement with those of anhydrous single crystal olivine, albite, K-Na feldspar solid solution reported by Xu et al. (2000a) and Hu et al. (2011, 2013) in terms of negative pressure dependences, and however, there exist some different pressure dependences of silicate perovskite and ilmenite at lower mantle conditions reported by Shankland et al. (1993), Katsura et al. (1998) and Zhang et al. (2006) in terms of positive pressure dependences, respectively. The electrical conductivity of almandine-rich garnet decrease with increasing pressure is due to more difficult formation of vacancies at high pressure.

Fig. 8 shows the relationship between electrical conductivity and oxygen fugacity at 3.0 GPa over the temperature range of 873 to 1273 K and corresponding to five different oxygen buffers including

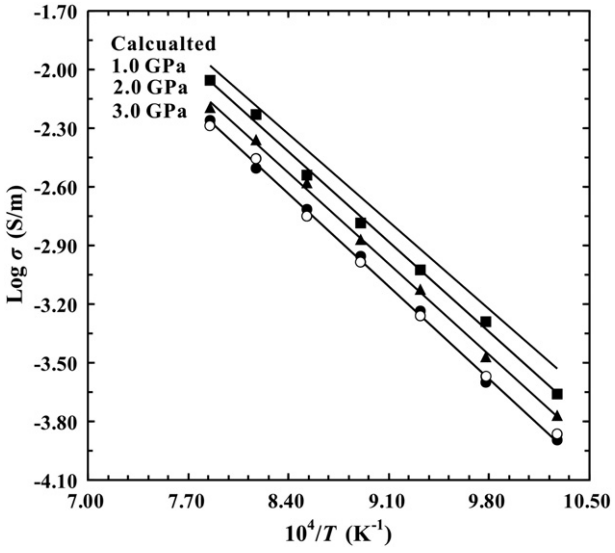

Fig. 7. Logarithm of electrical conductivity versus reciprocal temperature for the almandine-rich garnet under conditions of 1.0-3.0 GPa and with a NNO oxygen buffer. The open circles represent the conductivity of sample during the period of heating cycles at 3.0 GPa. The calculated electrical conductivity of almandine-rich garnet at atmospheric pressure is also shown by virtue of parameters of the Arrhenius relation.

Table 2
Fitted parameters of Arrhenius relation for the electrical conductivity of almandine-rich garnet.

Run No.	Oxygen buffers	P (GPa)	T (K)	Log σ_0	$\triangle H$ (eV)	R^2	$\triangle U$ (eV)	$\triangle V$ (cm^3/mol)
DL114	NNO	1.0	973-1273	3.11	1.31	0.9952	1.29 ±	2.01 ±
DL119	NNO	2.0	973-1273	3.06	1.34	0.9930	0.12	0.57
DL127	NNO	3.0	973-1273	3.04	1.35	0.9987		

$Fe_3O_4 + Fe_2O_3$, Ni + NiO, Fe + Fe_3O_4, Fe + FeO and Mo + MoO_2. At a given pressure of 3.0 GPa, the relation between the electrical conductivity of anhydrous samples and oxygen fugacity can be described as:

$$\mathrm{Log}_{10}\sigma = (2.67 \pm 0.05) + (0.054 \pm 0.003) \times \log_{10} f_{O_2} + \frac{(-5446 \pm 68)}{T} \quad (12)$$

The oxygen fugacity exponent (q) is 0.054 ± 0.003. We interpret this result assuming that the oxygen fugacity dependence of electrical conductivity is due to the dependence of number density of charge carrier on oxygen fugacity. The defect chemistry of anhydrous almandine-rich garnet indicates that the concentration of the ferric iron-related defects [X] depends on the chemical environment as:

$$[X] \propto f_{O_2}^{q} \times \alpha_{MeO}^{s} \quad (13)$$

where q and s are constants that are dependent on different defect types; f_{O_2} is the oxygen fugacity; α is the ionic activity, and MeO is the metal oxide. Similar to other dominant rock-forming minerals such as dry wadsleyite and ringwoodite in the transition zone (Huang et al., 2005), the values of q and s for typical defects of anhydrous almandine-rich garnet are summarized in Table 3.

The observed values of exponential factors of q (0.054) are very close to the exponents (0.061) obtained by Dai et al. (2012) for dry pyrope-rich garnet at conditions of 1.0-4.0 GPa, 873–1273 K, and controlled oxygen buffers ($Fe_3O_4 + Fe_2O_3$, Ni + NiO, Fe + Fe_3O_4, Fe + FeO and Mo + MoO_2). And it is very close to the results (0.050) obtained by Dai and Karato (2009b) for dry wadsleyite in the mantle transition zone under conditions of 15 GPa, 873–1273 K, and with three solid buffers (Ni + NiO, Mo + MoO_2 and Re + ReO_2). However, it is substantially lower than the exponent of 0.182 determined by Constable and Duba (1990); Constable et al. (1992); Constable and Roberts, 1997; Constable and Duba, 2002) for dry San Carlos olivine, Red Sea olivine, dunite and lherzolite under conditions of atmospheric pressure, temperature of 873–1773 K and controlled oxygen fugacity by continuously changing a ratio mixture of CO + CO_2 gas buffer across sample cavity. Karato and Wang (2013) recently put forward and developed the novel models for the concentration of point defects in olivine $(Mg,Fe)_2SiO_4$ or orthopyroxene $(Mg,Fe)SiO_3$, depending on the chemical environment under chemically neutral conditions for either $\left[Fe_{Mg}^{\bullet}\right] = \left[H_{Mg}^{'}\right]$ ($p = 1/4$, $q = 1/8$, and $r = -1/2$) or $\left[Fe_{Mg}^{\bullet}\right] = \left[V_{Mg}^{''}\right]$ ($p = 0$, $q = 1/6$, and $r = -1/3$). However, the value of q (0.054) for almandine-rich garnet is less than simple model predicted, suggesting the involvement of other charge neutrality conditions, such as $[Fe_{Mg}^{\bullet}] = [V_O^{\bullet\bullet}]$ ($p = 0$, $q = -1/6$, and $r = 1/3$) and $[Fe_{Mg}^{\bullet}] = [e']$ ($p = 0$, $q = -1/6$, and $r = -2/3$), or that chemical equilibrium was only partially obtained.

In summary, all of above listed evidences including the activation energy (ΔU) 1.29 ± 0.12 eV, the activation volume (ΔV) 2.01 ± 0.57 cm^3/mol, the negative dependence of electrical conductivity on pressure, and as well as the positive dependence of electrical conductivity on oxygen fugacity make it clear that in our experiment the main electrical conduction mechanism of anhydrous almandine-rich garnet is the $Fe^{2+} \rightarrow Fe^{3+}$ hopping of small polaron, which is in general agreement with those of dry Fe-bearing silicates such as olivine, orthopyroxene, clinopyroxene, augite, pyrope-rich garnet, wadsleyite, and ringwoodite that previously reported dominantly representative minerals in the Earth crust, upper-mantle and transition zone (Dai et al., 2008a, b, 2010; Huang et al., 2005; Wang et al., 2006; Xu et al., 2000a; Yang, 2012; Yang and Heidelbach, 2012; Yang and McCammon, 2012; Yang et al., 2011; Yang et al., 2012; Zhang et al., 2012). Because the electrical conductivity of dry garnet shows a positive relation with the concentration of point defects, the electrical conductivity increases with a higher oxygen fugacity and a higher concentration of small polaron arising from a point defect reaction. At a typical temperature and pressure in the upper mantle, the influence of oxygen fugacity is substantial. Fig. 9

We compare the electrical conductivity of almandine-rich garnet with those of previously available results. The comparison is made at 3.0 GPa and for the same oxygen fugacity controlled by a Mo + MoO_2 buffer. The results show that under anhydrous (water-free) conditions, the almandine-rich garnet ($Alm_{82}Py_{15}Grs_3$) has about 3 times higher conductivity than pyrope ($Py_{73}Alm_{14}Grs_{13}$) by Dai and Karato (2009a). As argued by Romano et al. (2006), they investigated the electrical conductivity of synthetic pyrope ($Mg_3Al_2Si_3O_{12}$)–almandine ($Fe_3Al_2Si_3O_{12}$) samples and found that electrical conductivity increases by four orders of magnitude from $Py_{85}Alm_{15}$ to $Py_{20}Alm_{80}$. It has been suggested that the explanation of this discrepancy is due to the garnets investigated by Romano et al. (2006) containing a large amount of water, which would have produced anomaly high electrical conductivity,

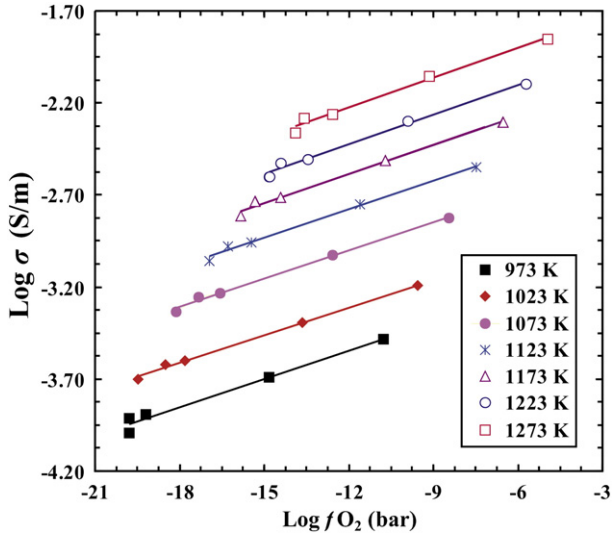

Fig. 8. Effect of oxygen fugacity on electrical conductivity of almandine-rich garnet under conditions of 3.0 GPa, 973–1273 K and controlled oxygen buffers ($Fe_3O_4 + Fe_2O_3$, Ni + NiO, Fe + Fe_3O_4, Fe + FeO and Mo + MoO_2).

Table 3
Point defect concentrations for dry almandine-rich garnet.

Defect	q	s	Defect	q	s
$[Si_i^{\bullet\bullet\bullet\bullet}]$	$-\frac{1}{3}$	$-\frac{10}{3}$	$[V_O^{\bullet\bullet}]$	$-\frac{1}{6}$	$-\frac{2}{3}$
$\left[V_M^{''}\right]$	$\frac{1}{6}$	$-\frac{1}{3}$	$\left[V_{Si}^{''''}\right]$	$\frac{1}{3}$	$\frac{10}{3}$
$[Mg_i^{\bullet\bullet}]$	$-\frac{1}{6}$	$\frac{1}{3}$	$[h^{\bullet}]$	$\frac{1}{6}$	$-\frac{1}{3}$
$[O_i^{''}]$	$\frac{1}{6}$	$\frac{2}{3}$	$[e']$	$-\frac{1}{6}$	$\frac{1}{3}$
$[Fe_{Mg}^{\bullet}]$	$\frac{1}{6}$	$-\frac{1}{3}$			

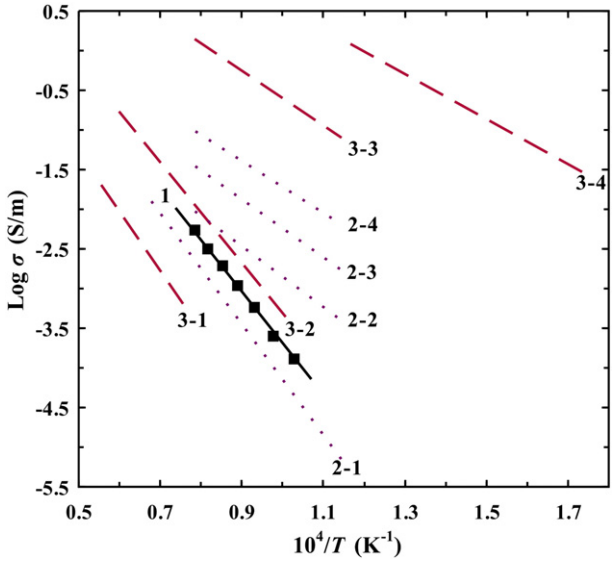

Fig. 9. Electrical conductivities of dry almandine-rich garnet (black solid lines) in this study compared with the previous results. Lines are indicated as follows: 1. Present study; 2–1, 2–2, 2–3 and 2–4 represent electrical conductivities of dry and hydrous pyrope-rich ($Py_{73}Alm_{14}Grs_{13}$) by Dai and Karato (2009a); 3–1, 3–2, 3–3 and 3–4 represent electrical conductivities of chemical compositions from $Py_{85}Alm_{15}$ to $Py_{20}Alm_{80}$ garnets by Romano et al. (2006). Comparison is made at P = 3 GPa and for the same oxygen fugacity controlled by a Mo + MoO_2 buffer.

especially in the low-temperature region (Dai et al., 2012; Yang et al., 2012). The actual contribution from almandine-rich garnet depends on not only its volume percentage but also its geometry. Although the dry almandine-rich garnet has a relatively higher conductivity than those of dominant dry rock-forming minerals such as olivine and pyroxene in the upper mantle, there exists an extremely feeble effect on the bulk conductivity because almandine-rich garnet is a relatively rare mineral phase in the cal-alkaline volcanic rocks worldwide and is impossibly interconnected. In brief, for a small quantity of volume percentage of almandine-rich garnet, its contribution is extremely feeble in a typical upper mantle and the transition zone of the Earth's mantle, but maybe its contribution becomes very important in the Central Slovakian Volcanic Filed (CSVF), the volcanic complexes of the Börzsöny and Visegrád Mts and the Cserhát and Mátra cal-alkaline volcanic rocks of the North Pannonian Basin in Eastern-Central Europe since almandine-rich garnet is relatively common (Harangi et al., 2001).

Acknowledgements

We thank the editor of Professor Mian Liu and two anonymous reviewers for their very constructive comments and suggestions in the reviewing process, which helped us greatly in improving the manuscript. The enlightening discussions were conducted with Professor Shun-ichiro Karato from Department of Geology and Geophysics, Yale University, USA. Dr Robert Farla, George Amulele and Zhenting Jiang in Karato's high-pressure laboratory kindly provided technical guidance and assistance in the FT-IR measurement. This research was financially supported by the "135" Program of Institute of Geochemistry, CAS and NSF of China (41174079, 40974051 and 40704010).

References

Bagdassarov, N., 2011. Phase transitions in $CsHSO_4$ up to 2.5 GPa: impedance spectroscopy under pressure. Journal of Physics and Chemistry of Solids 72, 236–244.
Bagdassarov, N., Kopylova, M., Eichert, S., 2007. Laboratory derived constraints on electrical conductivity beneath Slave craton. Physics of the Earth and Planetary Interiors 161, 126–133.
Bagdassarov, N., Batalev, V., Egorova, V., 2011. State of lithosphere beneath Tien Shan from petrology and electrical conductivity of xenoliths. Journal of Geophysical Research 116, B01202. http://dx.doi.org/10.1029/2009JB007125.
Chou, I.M., 1978. Calibration of oxygen buffers at elevated P and T using the hydrogen fugacity sensor. American Mineralogist 63, 690–703.
Chou, I.M., Eugster, H.P., 1976. Fugacity control and dissociation constants of HBr and HI. Contributions to Mineralogy and Petrology 56, 77–100.
Constable, S., Duba, A., 1990. Electrical conductivity of olivine, a dunite, and the mantle. Journal of Geophysical Research 95, 6967–6978.
Constable, S., Duba, A., 2002. Diffusion and mobility of electrically conducting defects in olivine. Physics and Chemistry of Minerals 29, 446–454.
Constable, S., Roberts, J.J., 1997. Simultaneous modeling of thermopower and electrical conduction in olivine. Physics and Chemistry of Minerals 24, 319–325.
Constable, S., Shankland, T.J., Duba, A., 1992. The electrical conductivity of an isotropic olivine mantle. Journal of Geophysical Research 97, 3397–3404.
Dai, L., Karato, S., 2009a. Electrical conductivity of pyrope-rich garnet at high temperature and high pressure. Physics of the Earth and Planetary Interiors 176, 83–88.
Dai, L., Karato, S., 2009b. Electrical conductivity of wadsleyite at high temperatures and high pressures. Earth and Planetary Science Letters 287, 277–283.
Dai, L., Karato, S., 2009c. Electrical conductivity of orthopyroxene: implications for the water content of the asthenosphere. Proceedings of the Japan Academy Series B-Physical and Biological Sciences 85, 466–475.
Dai, L., Li, H., Hu, H., Shan, S., 2008a. Experimental study of grain boundary electrical conductivities of dry synthetic peridotite under high-temperature, high-pressure, and different oxygen fugacity conditions. Journal of Geophysical Research 113, B12211. http://dx.doi.org/10.1029/2008JB005820.
Dai, L., Li, H., Deng, H., Liu, C., Su, G., Shan, S., Zhang, L., Wang, R., 2008b. In situ control of different oxygen fugacity experimental study on the electrical conductivity of lherzolite at high temperature and high pressure. Journal of Physics and Chemistry of Solids 69, 101–110.
Dai, L., Li, H., Hu, H., Shan, S., 2009. Novel technique to control oxygen fugacity during high-pressure measurements of grain boundary conductivities of rocks. The Review of Scientific Instruments 80, 033903. http://dx.doi.org/10.1063/1.3097882.
Dai, L., Li, H., Li, C., Hu, H., Shan, S., 2010. The electrical conductivity of dry polycrystalline olivine compacts at high temperatures and pressures. Mineralogical Magazine 74, 849–857.
Dai, L., Li, H., Hu, H., Shan, S., Jiang, J., Hui, K., 2012. The effect of chemical composition and oxygen fugacity on the electrical conductivity of dry and hydrous garnet at high temperatures and pressures. Contributions to Mineralogy and Petrology 163, 689–700.
Du Frane, W.L., Tyburczy, J.A., 2012. Deuterium–hydrogen exchange in olivine: implications for point defects and electrical conductivity. Geochemistry Geophysics Geosystem 13, Q03004. http://dx.doi.org/10.1029/2011GC003895.
Du Frane, W.L., Roberts, J.J., Toffelmier, D.A., Tyburczy, J.A., 2005. Anisotropy of electrical conductivity in dry olivine. Geophysical Research Letters 32, L24315. http://dx.doi.org/10.1029/2005GL023879.
Evans, R.L., 2012. Earth's electromagnetic environment, 3A.Conductivity of Earth material. In: Chave, A.D., Duba, A.G. (Eds.), The magnetotelluric method, theory and practice. Cambridge University Press, pp. 50–95.
Ferri, F., Gibert, B., Violay, M., Cesare, B., 2013. Electrical conductivity in a partially molten crust from measurements on metasedimentary enclaves. Tectonophysics 586, 84–94.
Frost, D.J., McCammon, C., 2008. The redox state of Earth's mantle. Annual Review of Earth and Planetary Sciences 36, 389–420.
Fuji-ta, K., Katsura, T., Tainosho, Y., 2004. Electrical conductivity measurement of granulite under mid- to lower crustal pressure-temperature conditions. Geophysical Journal International 157, 79–86.
Fuji-ta, K., Katsura, T., Matsuzaki, T., Ichiki, M., Kobayashi, T., 2007a. Electrical conductivity measurement of gneiss under mid- to lower crustal P-T conditions. Tectonophysics 434, 93–101.
Fuji-ta, K., Katsura, T., Matsuzaki, T., Ichiki, M., 2007b. Electrical conductivity measurements of brucite under crustal pressure and temperature conditions. Earth, Planets and Space 59, 645–648.
Fuji-ta, K., Katsura, T., Ichiki, M., Matsuzaki, T., Kobayashi, T., 2011. Variations in electrical conductivity of rocks above metamorphic conditions. Tectonophysics 504, 116–121.
Gaillard, F., Malki, M., Iacono-Marziano, G., Pichavant, M., Scaillet, B., 2008. Carbonatite melts and electrical conductivity in the asthenosphere. Science 322, 1363–1365.
Harangi, S.Z., Downes, H., Kósa, L., Szabó, C.S., Thirlwall, M.F., Mason, F.R.D., Mattey, D., 2001. Almandine garnet in calc-alkaline basin (Eastern-Central Europe): geochemistry, petrogenesis and geodynamic implications. Journal of Petrology 42, 1813–1843.
Hu, H., Li, H., Dai, L., Shan, S., Zhu, C., 2011. Electrical conductivity of albite at high temperatures and high pressures. American Mineralogist 96, 1821–1827.
Hu, H., Li, H., Dai, L., Shan, S., Zhu, C., 2013. Electrical conductivity of alkali feldspar solid solutions at high temperatures and high pressures. Physics and Chemistry of Minerals 40, 51–62.
Huang, X., Xu, Y., Karato, S., 2005. Water content of the mantle transition zone from the electrical conductivity of wadsleyite and ringwoodite. Nature 434, 746–749.
Huang, X., Xu, Y., Karato, S., 2006. A wet mantle conductor? Nature 439, E3–E4.
Jones, A.G., Evans, R.L., Eaton, D.W., 2009. Velocity-conductivity relationships for mantle mineral assemblages in Archean cratonic lithosphere based on a review of laboratory data and Hashin-Shtrikman extremal bounds. Lithos 109, 131–143.
Jones, A.G., Fullea, J., Evans, R.L., Muller, M.R., 2012. Water in cratonic lithosphere: calibrating laboratory-determined models of electrical conductivity of mantle minerals using geophysical and petrological observations. Geochemistry Geophysics Geosystems 13, Q06010. http://dx.doi.org/10.1029/2012GC004055.

Karato, S., 2011a. Water distribution across the mantle transition zone and its implications for global material circulation. Earth and Planetary Science Letters 301, 413–423.
Karato, S., 2011b. Some issues on the strength of the lithosphere. Journal of Earth Sciences 22, 131–136.
Karato, S., Dai, L., 2009. Comments on "Electrical conductivity of wadsleyite as a function of temperature and water content" by Manthilake et al. Physics of the Earth and Planetary Interiors 174, 19–21.
Karato, S., Wang, D., 2013. Electrical conductivity of minerals and rocks. In: Karato, S., Wiley, John, Hoboken, N.J. (Eds.), Physics and Chemistry of the Deep Earth, pp. 1–144.
Katsura, T., Sato, K., Ito, E., 1998. Electrical conductivity of silicate perovskite at lower-mantle conditions. Nature 395, 493–495.
Kavner, A., Li, X., Jeanloz, R., 1995. Electrical conductivity of a natural (Mg, Fe)SiO3 majorite garnet. Geophysical Research Letters 22, 3103–3106.
Kelbert, A., Schultz, A., Egbert, G., 2009. Global electromagnetic induction constraints on transition-zone water content variations. Nature 460, 1003–1006.
Laštovičková, M., 1991. A review of laboratory measurements of the electrical conductivity of rocks and minerals. Physics of the Earth and Planetary Interiors 66, 1–11.
Liu, Y., Xie, H., Zhou, W., Guo, J., 2002. A method for experimental determination of compressional velocities in rocks and minerals at high pressure and high temperature. Journal of Physics: Condensed Matter 14, 11381–11384.
McCammon, C., Frost, D.J., Smyth, J.R., Laustsen, H.M.S., Kawamoto, T., Ross, N.L., van Aken, P.A., 2004. Oxidation state of iron in hydrous mantle phases: implications for subduction and mantle oxygen fugacity. Physics of the Earth and Planetary Interiors 143–144, 157–169.
Mookherjee, M., Karato, S., 2010. Solubility of water in pyrope-rich garnet at high pressures and temperature. Geophysical Research Letters 37, L03310. http://dx.doi.org/10.1029/2009GL041289.
Ni, H., Keppler, H., Manthilake, M.A.G.M., Katsura, T., 2011a. Electrical conductivity of dry and hydrous $NaAlSi_3O_8$ glasses and liquids at high pressures. Contributions to Mineralogy and Petrology 162, 501–513.
Ni, H., Keppler, H., Behrens, H., 2011b. Electrical conductivity of hydrous basaltic melts: implications for partial melting in the upper mantle. Contributions to Mineralogy and Petrology 162, 637–650.
Nover, G., 2005. Electrical properties of crustal and mantle rocks-a review of laboratory measurements and their explanation. Surveys in Geophysics 26, 593–651.
Paterson, M.S., 1982. The determination of hydroxyl by infrared absorption in quartz, silicate glasses and similar materials. Bulletin de Mineralogie 105, 20–29.
Poe, B.T., Romano, C., Nestola, F., Smyth, J.R., 2010. Electrical conductivity anisotropy of dry and hydrous olivine at 8 GPa. Physics of the Earth and Planetary Interiors 181, 103–111.
Poe, B.T., Romano, C., Di Genova, D., Behrens, H., Scarlato, P., 2012. Mixed electrical conduction in a hydrous pantellerite glass. Chemical Geology 320–321, 140–146.
Pommier, A., 2013. Interpretation of magnetotelluric results using laboratory measurements. Surv Geophys. http://dx.doi.org/10.1007/s10712-013-9226-2 (in press).
Pommier, A., Le-Trong, E., 2011. "SIGMELTS": a web portal for electrical conductivity calculations in geosciences. Computers & Geosciences 37, 1450–1459.
Pommier, A., Gaillard, F., Pichavant, M., 2010a. Time-dependent changes of the electrical conductivity of basaltic melts with redox state. Geochimica et Cosmochimica Acta 74, 1653–1671.
Pommier, A., Gaillard, F., Malki, M., Pichavant, M., 2010b. Methodological re-evaluation of the electrical conductivity of silicate melts. American Mineralogist 95, 284–291.
Roberts, J.J., Duba, A.G., 1995. Transient electrical response of San Quintin dunite as a function of oxygen fugacity changes: information about charge carriers. Geophysical Research Letters 22, 453–456.
Roberts, J.J., Tyburczy, J.A., 1991. Frequency dependent electrical properties of polycrystalline olivine compacts. Journal of Geophysical Research 96, 16205–16222.
Roberts, J.J., Tyburczy, J.A., 1993a. Impedance spectroscopy of single and polycrystalline olivine: evidence for grain boundary transport. Physics and Chemistry of Minerals 20, 19–26.
Roberts, J.J., Tyburczy, J.A., 1993b. Frequency dependent electrical properties of dunite as functions of temperature and oxygen fugacity. Physics and Chemistry of Minerals 19, 545–561.
Roberts, J.J., Tyburczy, J.A., 1994. Frequency dependent electrical properties of minerals and partial-melts. Survey in Geophysics 15, 239–262.
Roberts, J.J., Kinney, J.H., Siebert, J., Ryerson, F.J., 2007. Fe-Ni-S melt permeability in olivine: implications for planetary core formation. Geophysical Research Letters 34, L14306. http://dx.doi.org/10.1029/2007GL030497.
Romano, C., Poe, B.T., Kreidie, N., McCammon, C., 2006. Electrical conductivities of pyrope-almandine garnets up to 19 GPa and 1700 °C. American Mineralogist 91, 1371–1377.
Romano, C., Poe, B.T., Tyburczy, J.A., Nestola, F., 2009. Electrical conductivity of hydrous wadsleyite. European Journal of Mineralogy 21, 615–622.
Selway, K., 2013. On the causes of electrical conductivity anomalies in tectonically stable lithosphere. Surv Geophys. http://dx.doi.org/10.1007/s10712-013-9235-1 (in press).
Shankland, T.J., Peyronneau, J., Poirier, J.P., 1993. Electrical conductivity of the Earth's lower mantle. Nature 366, 453–455.
Tyburczy, J.A., Roberts, J.J., 1990. Low frequency electrical response of polycrystalline olivine compacts: grain boundary transport. Geophysical Research Letters 17, 1985–1988.
Wang, D., Karato, S., 2013. Electrical conductivity of talc aggregates at 0.5 GPa: influence of dehydration. Physics and Chemistry of Minerals 40, 11–17.
Wang, D., Mookherjee, M., Xu, Y., Karato, S., 2006. The effect of water on the electrical conductivity of olivine. Nature 443, 977–980.
Wang, D., Li, H., Yi, L., Shi, B., 2008. The electrical conductivity of upper-mantle rocks: water content in the upper mantle. Physics and Chemistry of Minerals 35, 157–162.
Wang, D., Li, H., Yi, L., Matsuzaki, T., Yoshino, T., 2010. Anisotropy of synthetic quartz electrical conductivity at high pressure and temperature. Journal of Geophysical Research 115, B09211. http://dx.doi.org/10.1029/2009JB006695.
Xu, Y., McCammon, C., 2002. Evidence for ionic conductivity in lower mantle (Mg,Fe)(Si,Al)O_3 perovskite. Journal of Geophysical Research 107, B102251. http://dx.doi.org/10.1029/2001JB000677.
Xu, Y., Shankland, T.J., 1999. Electrical conductivity of orthopyroxene and its high-pressure phases. Geophysical Research Letters 26, 2645–2648.
Xu, J., Zhang, Y., Hou, W., Xu, H., Guo, J., Wang, Z., Zhao, H., Wang, R., Huang, E., Xie, H., 1994. Measurements of ultrasonic wave velocities at high temperature and high pressure for window glass, pyrophyllite, and kimberlite up to 1400 °C and 5.5 GPa. High temperatures high pressures 26, 375–384.
Xu, Y., Poe, B.T., Shankland, T.J., Rubie, D.C., 1998a. Electrical conductivity of olivine, wadsleyite, and ringwoodite under upper-mantle conditions. Science 280, 1415–1418.
Xu, Y., McCammon, C., Poe, B.T., 1998b. The effect of alumina on the electrical conductivity of silicate perovskite. Science 282, 922–924.
Xu, Y., Shankland, T.J., Duba, A.G., 2000a. Pressure effect on electrical conductivity of mantle olivine. Physics of the Earth and Planetary Interiors 118, 149–161.
Xu, Y., Shankland, T.J., Poe, B.T., 2000b. Laboratory-based electrical conductivity in the earth's mantle. Journal of Geophysical Research 105, 27865–27875.
Yang, X., 2011. Origin of high electrical conductivity in the lower continental crust: a review. Survey in Geophysics 32, 875–903.
Yang, X., 2012. Orientation-related electrical conductivity of hydrous olivine, clinopyroxene and plagioclase and implications for the structure of the lower continental crust and uppermost mantle. Earth and Planetary Science Letters 317–318, 241–250.
Yang, X., Heidelbach, F., 2012. Grain size effect on the electrical conductivity of clinopyroxene. Contributions to Mineralogy and Petrology 163, 939–947.
Yang, X., McCammon, C., 2012. Fe^{3+}-rich augite and high electrical conductivity in the deep lithosphere. Geology 40, 131–134.
Yang, X., Keppler, H., McCammon, C., Ni, H., Xia, Q., Fan, Q., 2011. Effect of water on the electrical conductivity of lower crustal clinopyroxene. Journal of Geophysical Research 116, B04208. http://dx.doi.org/10.1029/2010JB008010.
Yang, X., Keppler, H., McCammon, C., Ni, H., 2012. Electrical conductivity of orthopyroxene and plagioclase in the lower crust. Contributions to Mineralogy and Petrology 63, 33–48.
Yoshino, T., 2010. Laboratory electrical conductivity measurement of mantle minerals. Survey in Geophysics 31, 163–206.
Zhang, B., Katsura, T., Shatskiy, A., Matsuzaki, T., Wu, X., 2006. Electrical conductivity of $FeTiO_3$ ilmenite at high temperature and high pressure. Physical Review B 73, 134014 (10.113/PhysRevB.73.134104).
Zhang, B., Yoshino, T., Wu, X., Matsuzaki, T., Shan, S.M., Katsura, T., 2012. Electrical conductivity of enstatite as a function of water content: implications for the electrical structure in the upper mantle. Earth and Planetary Science Letters 357–358, 11–20.
Zhou, W., Fan, D., Liu, Y., Xie, H., 2011. Measurements of wave velocity and electrical conductivity of an amphibolite from southwestern margin of the Tarim Basin at pressures to 1.0 GPa and temperatures to 700 ° C: comparison with field observations. Geophysical Journal International 187, 1393–1404.